

Novel Cosmic-Ray Electron and Positron Constraints on MeV Dark Matter Particles

Mathieu Boudaud,^{1,2,*} Julien Lavalle,^{3,†} and Pierre Salati^{1,‡}

¹LAPTh, Université Savoie Mont Blanc & CNRS,

9 Chemin de Bellevue, B.P.110, F-74941 Annecy-le-Vieux – France

²Laboratoire de Physique Théorique et Hautes Energies (LPTHE),
UMR 7589 CNRS & UPMC, 4 Place Jussieu, F-75252 Paris – France

³Laboratoire Univers & Particules de Montpellier (LUPM),

CNRS & Université de Montpellier (UMR-5299),

Place Eugène Bataillon, F-34095 Montpellier Cedex 05 – France

MeV dark matter (DM) particles annihilating or decaying to electron-positron pairs cannot, in principle, be observed via local cosmic-ray (CR) measurements because of the shielding solar magnetic field. In this letter, we take advantage of spacecraft Voyager 1’s capacity for detecting interstellar CRs since it crossed the heliopause in 2012. This opens up a new avenue to probe DM in the sub-GeV energy/mass range that we exploit here for the first time. From a complete description of the transport of electrons and positrons at low energy, we derive predictions for both the secondary astrophysical background and the pair production mechanisms relevant to DM annihilation or decay down to the MeV mass range. Interestingly, we show that reacceleration may push positrons up to energies larger than the DM particle mass. We combine the constraints from the Voyager and AMS-02 data to get novel limits covering a very extended DM particle mass range, from MeV to TeV. In the MeV mass range, our limits reach annihilation cross sections of order $\langle\sigma v\rangle \sim 10^{-28} \text{cm}^3/\text{s}$. An interesting aspect is that these limits barely depend on the details of cosmic-ray propagation in the weak reacceleration case, a configuration which seems to be favored by the most recent boron-to-carbon (B/C) data. Though extracted from a completely different and new probe, these bounds have a strength similar to those obtained with the cosmic microwave background — they are even more stringent for p -wave annihilation.

PACS numbers: 12.60.-i,95.35.+d,96.50.S-,98.35.Gi,98.70.Sa

Thermally produced sub-GeV dark matter (DM) particles have triggered interest since the nonbaryonic particle DM proposal itself, including the weakly interacting massive particle (WIMP) paradigm (*e.g.* [1]). Allowed scenarios involve DM particle masses m_χ larger than a few keV (warm DM – WDM), usually bounded by structure formation [2–5]. In the MeV mass range, thermal DM candidates are already cold enough not to differ from cold DM (CDM) structure formation on scales of dwarf galaxies. However, if they have remained coupled to radiation or neutrinos sufficiently long, an oscillatory damping pattern in the structure power spectrum could be observed on small scales that differs from the standard free-streaming cutoff of WDM [6, 7], and alleviate the too-big-to-fail problem affecting the CDM paradigm on small scales [8]. Besides, self-interacting DM scenarios could be achieved from the thermal freeze out of particles in the MeV mass range [9], as well as strongly interacting DM [10], which may also cure small scale issues in structure formation. Overall, many efforts are now devoted to probe this mass range through direct and indirect searches (see *e.g.* [11]).

Astrophysical observations already constrain MeV DM candidates. For instance, gamma-ray measurements

generically constrain MeV candidates, depending on assumptions on the shape of the inner Galactic halo profile [12, 13]. Heating of the plasma at the CMB decoupling time is also constrained by current observations and actually allows us to get stringent bounds on MeV annihilating or decaying DM [14–16], down to an s -wave annihilation cross section of $\langle\sigma v\rangle \lesssim 10^{-29} \text{cm}^3/\text{s}$ for the former case (assuming annihilation into electron-positron [e^\pm] pairs).

Less prone to uncertainties in the halo shape [17], cosmic-ray (CR) e^\pm s could provide independent probes of annihilation or decay of MeV DM. Nevertheless, interstellar sub-GeV e^\pm s are shielded by the solar magnetic field (the so-called solar modulation effect) [18, 19] such that they cannot reach detectors orbiting the Earth. In this Letter, we bypass this limitation by exploiting, for the first time in this context (see *e.g.* [20] for more conventional astrophysical aspects), the e^\pm data of the Voyager 1 spacecraft [21, 22]. Indeed, Voyager 1 has crossed the heliopause during the summer 2012, and, since then, has traveled through interstellar space. Since it is equipped with particle detectors, with one dedicated to e^\pm measurements (no discrimination between electrons and positrons), this opens up a new avenue for DM searches in the sub-GeV mass range. Here, we will use the e^\pm Voyager 1 data from the end of 2012, extracted after the calibration of response functions from simulations of the detector (most conservative dataset) and released in Ref. [22] – *i.e.* 4 data points in the $\sim 10 - 50$ MeV energy range with excellent statistics. This data set

* boudaud@lpthe.jussieu.fr

† lavalle@in2p3.fr

‡ pierre.salati@lupth.cnrs.fr

will be complemented at higher energy by the AMS-02 positron data [23], imported from the database proposed in [24].

The transport of CR e^\pm s in the Milky Way (MW) can be described by a general diffusion equation [25–31] that includes spatial diffusion, convection, reacceleration, and energy losses. We use the semianalytic method proposed in Ref. [32] to solve this equation. Solutions assume a plain diffusion over a cylindrical magnetic halo of radius R and half height L , with boundary conditions such that the CR density vanishes at the halo borders. Some processes are dominant in the thin Galactic disk, others extend to the whole magnetic halo. The first category includes diffusive reacceleration (featured by a pseudo-Alfvén velocity V_a), and energy losses due to electromagnetic interactions with the interstellar gas [$b_{\text{gas}}(E)$]. The second one includes spatial diffusion (with a scalar coefficient $K(\mathcal{R}) = \beta K_0(\mathcal{R}/1\text{GV})^\delta$, with $\mathcal{R} \equiv p/|q|$ the rigidity), convection (with velocity $\vec{V}_c = \text{sgn}(z) V_c \vec{e}_z$ of constant modulus), and higher-energy losses from inverse Compton and synchrotron emissions ($b(E)$). The technical difficulty in applying this method to e^\pm s comes from the fact that derivatives in the momentum space are not confined to the disk as is the case for nuclei, but high-energy losses, which dominate above ~ 10 GeV, are efficient all over the magnetic halo. This was addressed in an approximate way in Ref. [28], but recently solved in a systematic and elegant way in Ref. [31]. We therefore refer the reader to Ref. [31] for a thorough presentation of the propagation model we will further use in this Letter. Note that complementary full numerical approaches exist [33–35], which are qualitatively similar to ours.

For the propagation parameters, we consider large- L propagation models because low-energy positron data (0.1–2 GeV) severely constrain values of $L \lesssim 8$ kpc [31, 36], as do the latest B/C data [37]. More precisely, we use the Max model proposed in [32, 38] (model A henceforth: $L = 15$ kpc, $K_0 = 0.0765 \text{ kpc}^2/\text{Myr}$, $\delta = 0.46$, $V_a = 117.6 \text{ km/s}$, $V_c = 5 \text{ km/s}$), which lies at the border of the current positron bounds [31], together with the B/C best-fit model of Ref. [37] (model B: $L = 13.7$ kpc, $K_0 = 0.0967 \text{ kpc}^2/\text{Myr}$, $\delta = 0.408$, $V_a = 31.9 \text{ km/s}$, $V_c = 0.2 \text{ km/s}$). These models mostly differ in reacceleration, which is strong for model A (fitted on old B/C data), and weak for model B (most recent B/C data)¹. A full exploration of the parameter space goes beyond the scope of this Letter, but models A and B characterize the state-of-the-art description of Galactic CR propagation within a standard set of assumptions (isotropic and scalar spatial diffusion). We first compute the secondary e^\pm fluxes, *i.e.* e^\pm s generated from inelastic interactions between CR nuclei and the interstellar gas. Though conventional sources of primary CRs (*e.g.* pulsar winds, supernova remnants) contribute to the total

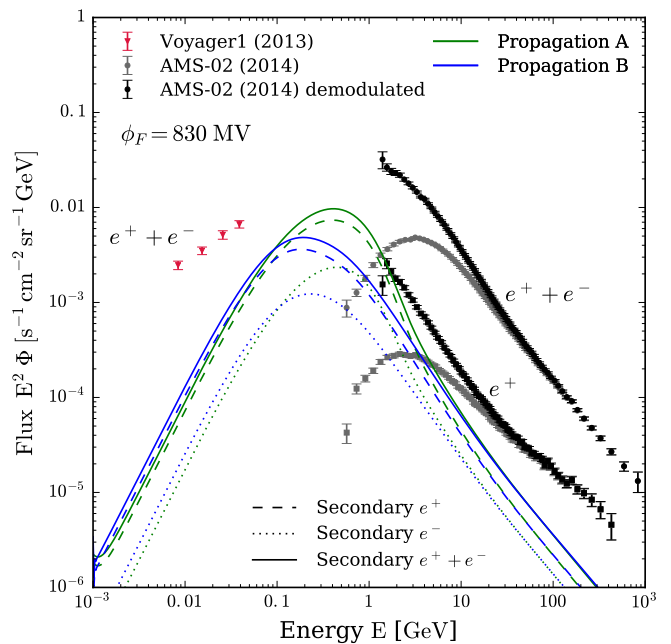


FIG. 1: CR e^\pm data from Voyager (red triangles) and AMS-02 (plain circles), and e^+ AMS-02 data (plain squares). The latter are demodulated with a Fisk potential of $\phi = 830$ MV. The curves show the interstellar secondary background predicted for propagation models A and B.

e^\pm fluxes [29, 30, 39, 40], we only consider the secondary background because large theoretical uncertainties affect this primary component [29, 30], placing our coming constraints on the conservative side. Our predictions for the interstellar flux are shown in Fig. 1 against the Voyager and AMS-02 data. For the latter, we demodulated the data (the Voyager data are modulation free). We proceed by using the force-field approximation [18, 41] with a Fisk potential ϕ in the range [724 MV, 830 MV] for the AMS-02 data-taking period (see [42]). From Fig. 1, we see that the secondary e^\pm s contribute significantly to the data only in the AMS-02 energy range and are negligible in the Voyager range. This has important consequences: not only are the Voyager data free of solar modulation, but they are also insensitive to the presence of secondaries. Besides, we can already notice from Fig. 1 the impact of reacceleration: the secondary e^\pm peak observed in $E^2\Phi_{e^\pm}$ is shifted to higher energy in the strong-reacceleration case (model A), which will make the AMS-02 data more constraining than in the weak-reacceleration case (model B). Because confined to the disk here, reacceleration in both models is consistent with the power constraints found in [43, 44]. Finally, it is worth pointing out that, surprisingly enough, the lowest AMS-02 energy point for the e^+ flux lies significantly lower than its neighbors, which may lead to very strong bound on DM annihilation or decay. To remain conservative, we remove it from our analysis.

We now compute the DM annihilation contributions

¹ The relevant (inverse) time scale is given by $V_a^2/K_0 \sim 0.2 \text{ Myr}^{-1}$ for model A (0.01 Myr^{-1} for model B).

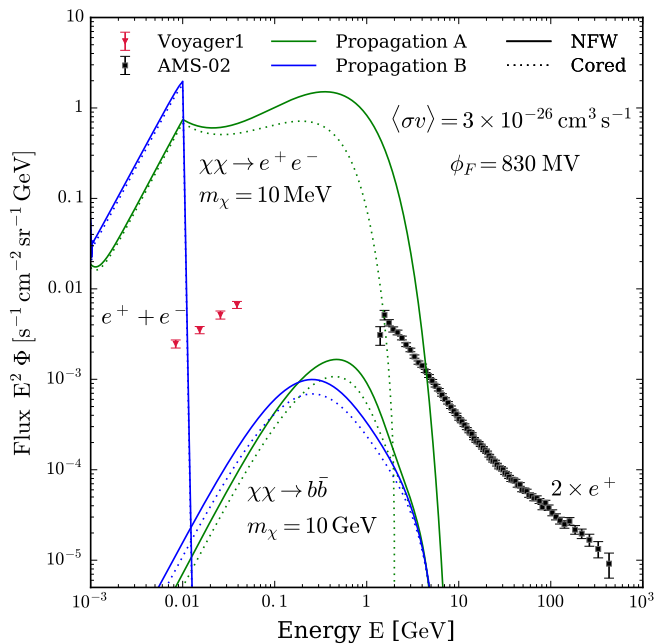


FIG. 2: Predictions (e^\pm) for 2 template cases: a 10 MeV WIMP annihilating into e^+e^- (+ FSR), and a 10 GeV WIMP annihilating into $b\bar{b}$. The data are the same as in Fig. 1, but the AMS-02 e^+ data is multiplied by a factor of 2 to compare with the e^\pm primaries. Propagation models A and B, and the NFW and cored DM halo models were used.

to these observables. We consider several channels and assume unity branching ratios: e^\pm , μ^\pm , τ^\pm , $b\bar{b}$, W^\pm . We generate injection spectra with the `MicroMEGAS` code [45], which includes final-state radiation (FSR) processes. For the DM halo profile, we assume two different spherical cases: a Navarro-Frenk-White halo [46] scaling like $1/r$ in the center (NFW halo henceforth), and a cored halo profile with constant central DM density (cored halo). We use the kinematically constrained halo parameters from Ref. [47], such that our halos are dynamically self-consistent. In both halos, the DM density at the solar position $r_\odot \simeq 8.2$ kpc is $\rho_\odot \simeq 0.4 \text{ GeV/cm}^3$.

Template predictions for the DM-induced e^\pm fluxes are shown in Fig. 2, considering WIMPs of 10 MeV (10 GeV) annihilating into e^+e^- ($b\bar{b}$). In both cases, e^+ s and e^- s share the same injection spectrum and the same propagation history, such that e^\pm predictions can be compared to the e^+ data by multiplying the latter by two. We reported our results for propagation models A and B, and for the NFW and cored halos. In the weak-reacceleration case (model A), the e^\pm flux is suppressed beyond the maximal injected energy set by m_χ , while in the strong-reacceleration case (model B), low-energy e^\pm s are reaccelerated beyond m_χ . This important feature of the strong-reacceleration regime has, to our knowledge, never been noticed before: DM-induced e^\pm s could then be observed beyond m_χ , which makes the GeV data also relevant to constrain sub-GeV DM.

Reacceleration also rules the impact of the DM halo shape. Without reacceleration, sub-GeV CR propagation is mostly governed by energy losses, such that e^\pm s injected at sub-GeV energies and coming from regions close to the Galactic center (GC) have been drifted to the low-energy part of the spectrum. This is illustrated in Fig. 2 for the e^+e^- channel, for which even if an NFW halo induces a larger annihilation rate at the GC, the net increase in the $E^2\Phi_{e^\pm}$ curve for model B is lost at low energies, while the peak at the WIMP mass only reflects the very local annihilation rate. For the $b\bar{b}$ channel, GeV e^\pm s injected at GeV energies in the GC are locally observed at sub-GeV energies, hence a larger flux for a cuspy halo. On the other hand, efficient reacceleration (model A) makes these e^\pm s continuously reheated as they cross the disk on their way to us, compensating for energy losses, such that the difference between an NFW and a cored halo is now more pronounced beyond m_χ (though still much less than the differences induced in gamma-ray predictions [17]). This non-trivial effect of reacceleration strengthens the complementarity of the low-energy Voyager data with the higher-energy AMS-02 data, the former (latter) providing significant constraints on predictions based upon weak-(strong-)reacceleration models.

The AMS-02 data are particularly constraining in the strong-reacceleration case, as secondary e^+ s provide a large contribution above 100 MeV (\sim the charged pion mass), while more sensitive to uncertainties in the solar modulation or V_a . In contrast, flux predictions in the sub-GeV range and in the weak-reacceleration regime are almost not sensitive to uncertainties in the other propagation parameters. This is because ionization energy losses are then the dominant process in the sub-GeV energy range (see Sect. A1). The corresponding rate b_{ion} scales like the local gas density, for which the uncertainties are small [48, 49]. In this configuration, the peak observed in $E^2\phi$ at the WIMP mass in the e^+e^- channel, whose amplitude fixes the Voyager bound on $\langle\sigma v\rangle$, is predicted to an excellent precision from the asymptotic approximation $\phi_{e^\pm}(E \rightarrow m_\chi) \rightarrow (v/4\pi)(\rho_\odot/m_\chi)^2\langle\sigma v\rangle/b_{\text{ion}}(E \rightarrow m_\chi)$.

We now combine the Voyager and AMS-02 data discussed above to derive limits on $\langle\sigma v\rangle$. We assume Majorana DM particles – a factor of 2 must be applied to our limits for Dirac fermions. We also assume that $\langle\sigma v\rangle$ is position independent (valid for an s -wave, approximate for a p -wave). We derive limits by adding our flux predictions for the primary and secondary components, and then demanding the total flux to lie below 2σ from each data point. These limits are displayed in Fig. 3. In the left panel, we specialize to the e^+e^- channel to illustrate differences due to propagation, solar modulation, and the DM halo shape. As already emphasized, the main variation is driven by reacceleration: weak-reacceleration models (\sim model B) are severely constrained by the Voyager data below ~ 100 MeV, with the nice bonus of not suffering from solar modulation. On the other

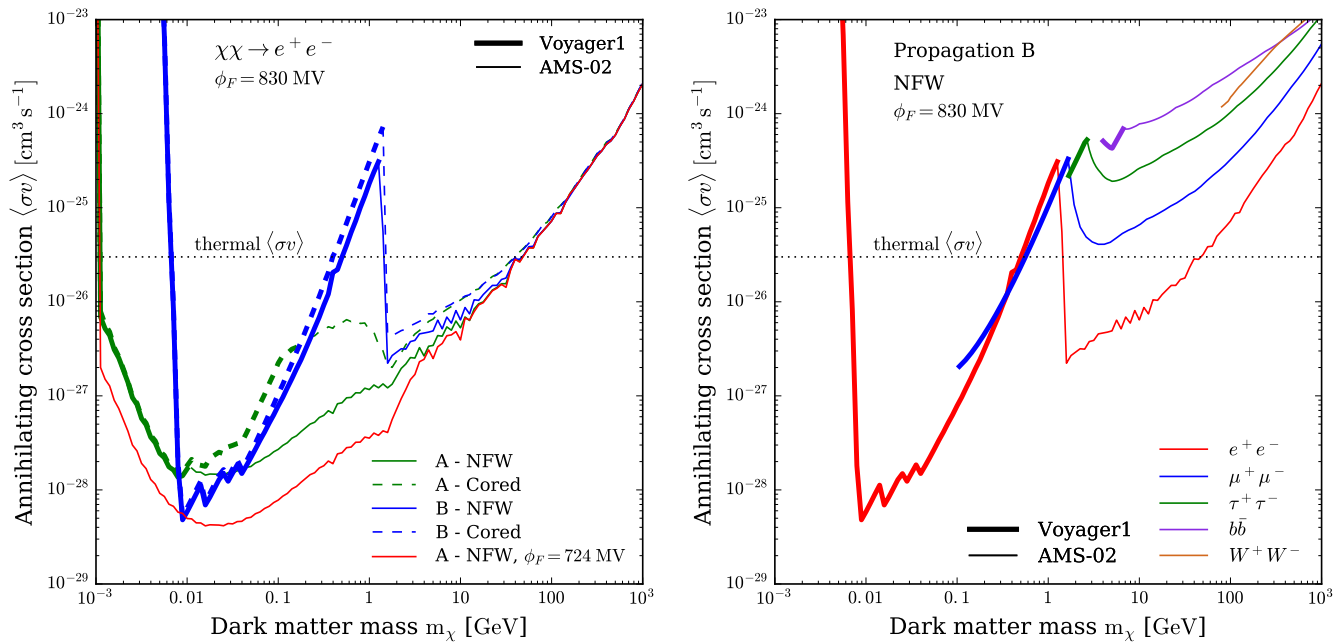


FIG. 3: Limits on $\langle\sigma v\rangle$ as a function of m_χ . Left: limits assuming annihilation into e^+e^- for propagation models A and B , and for the NFW and cored DM halos. A conservative solar modulation is set with $\phi = 830$ MV. The result for $\phi = 724$ MV is shown for the A -NFW configuration. Right: limits for different annihilation final states, assuming configuration B -NFW-830 MV.

hand, this regime makes it possible to “hide” a positron $E^2\Phi_{e^+}$ peak in the blind spot between the Voyager and AMS-02 datasets, such that the 0.1-1 GeV mass range becomes unconstrained. In contrast, strong-reacceleration models (\sim model A) forbid any blind spot, simply because sub-GeV e^\pm s are shifted up to GeV energies, in which case AMS-02 constraints are turned on – curves get then smoother over the full MeV-TeV energy range, with a transition below ~ 10 MeV where Voyager takes over. Limits inferred from strong-reacceleration models are also more sensitive to solar modulation, as illustrated by decreasing $\phi = 830$ MV to 724 MV: this justifies our conservative choice of 830 MV.

In the right panel of Fig. 3, we generalize our limits for several annihilation channels conservatively assuming propagation model B , $\phi = 830$ MV for the solar modulation of the AMS-02 data, and the NFW halo (closer to the best fit of [47] than the cored halo). These are our main results, which demonstrate for the first time that CR e^\pm s constrain annihilating DM down to the MeV mass range. We emphasize that for the e^+e^- channel our bound reaches $\langle\sigma v\rangle \sim 10^{-28} \text{ cm}^3/\text{s}$ in the 10-100 MeV mass range. We also notice the blind spot just below 1 GeV, but we stress that more reacceleration would fill in this spot again – future studies on propagation parameters will be crucial to settle this. At higher energy, we exclude thermal cross sections ($\sim 3 \times 10^{-26} \text{ cm}^3/\text{s}$) for masses up to ~ 50 GeV. This is less stringent than bounds obtained in Ref. [50], where the authors have assumed an additional primary component from pulsars

that saturates the data and forbids DM-induced contributions. Because of the large uncertainties affecting this primary component [29, 30], we have instead decided to discard it.

We now compare our results with those obtained from CMB analyses. In Ref. [16], limits on s -wave annihilation obtained for the e^+e^- channel go from $\langle\sigma v\rangle \lesssim 3 \times 10^{-30} \text{ cm}^3/\text{s}$ at 1 MeV up to $\sim 5 \times 10^{-29} \text{ cm}^3/\text{s}$ at 100 MeV, *i.e.* one order of magnitude better than ours. However, for p -wave annihilation, CMB limits degrade up to $\sim 10^{-24} \text{ cm}^3/\text{s}$ in the same mass range (derived assuming a velocity dispersion $\sigma_v = 100$ km/s). We can roughly convert our s -wave limits in terms of p -wave by assuming an isothermal velocity distribution for DM such that $\sigma_v^{\text{MW}} = v_c/\sqrt{2}$, where $v_c \simeq 240$ km/s is the local rotation velocity [51]. Therefore, our s -wave bounds $\langle\sigma v\rangle_{\text{max}}$ rescale to $\langle\sigma v\rangle_{\text{max}}(\sigma_v/\sigma_v^{\text{MW}})^2$ in terms of p -wave, giving $\sim 3 \times 10^{-29} \text{ cm}^3/\text{s}$ for $\sigma_v = 100$ km/s, *i.e.* an improvement by ~ 5 orders of magnitude. Finally, our bounds are slightly more stringent than those derived in gamma-ray studies [13], and less sensitive to the DM halo shape.

To conclude, we have considered for the first time the Voyager e^\pm data to derive constraints on annihilating MeV DM particles (decaying DM in Sect. A 2). Since Voyager has crossed the heliopause, solar modulation, which prevents MeV CRs to reach space experiments orbiting the Earth, can be evaded. We used state-of-the-art semianalytic methods to describe CR propagation, including all relevant processes. We considered constrained sets of propagation parameters featuring strong

(model *A*) and weak reacceleration (model *B*) to point out an interesting phenomenon: reacceleration may push e^\pm up to energies higher than m_χ in the sub-GeV mass range. Thus, GeV data become constraining also for DM particles in the sub-GeV mass range. We therefore combined the Voyager and AMS-02 datasets to derive constraints on DM annihilation, getting limits down to $\langle\sigma v\rangle \sim 10^{-28} \text{cm}^3/\text{s}$ at 10 MeV, quite competitive with respect to complementary gamma-ray studies, and less dependent on the halo shape. Other complementary CMB constraints are found more stringent for *s*-wave annihilation but less stringent by about five orders of magnitude for the *p*-wave. Finally, note that a similar analysis could apply to heavier DM particles with excited states separated by MeV gaps [52].

ACKNOWLEDGMENTS

We wish to thank Alan C. Cummings for valuable exchanges about the Voyager 1 data, and Martin Winkler for details about the B/C analysis made in Ref. [37]. We also thank the referees for their valuable comments which helped improve the presentation of our results. MB acknowledges support from the European Research Council (ERC) under the EU Seventh Framework Program (FP7/2007-2013)/ERC Starting Grant (agreement n. 278234 — NewDark project led by M. Cirelli). JL is partly supported by the OCEVU Labex (ANR-11-LABX-0060), the CNRS program *Défi InPhyNiTi*, and European Union’s Horizon 2020 research and innovation program under the Marie Skłodowska-Curie grant agreements No 690575 and No 674896 – in addition to recurrent funding by CNRS and Montpellier University. PS is partly supported by the Institut Universitaire de France (IUF).

Appendix A: Supplemental Material

1. Hierarchy in the propagation processes

In Fig. 4, we illustrate the time scales associated with the different processes at stake during the prop-

agation of e^\pm cosmic rays. All time scales are divided by the residence time scale in the disk, given by $\tau_{\text{disk}}(E) = hL/K(E)$, where h is the half-height of the thin gaseous disk (set to 100 pc) and L is the half-height of the Galactic magnetic halo. The strong-reacceleration regime (propagation model *A*) is shown in the left panel, while the weak-reacceleration regime (model *B*) is displayed in the right panel. In the latter, it is clear that not only does the ionization loss rate set the full energy loss rate ($1/\tau_I$) in the sub-GeV energy range, but it also dominates over the other processes. This makes the flux predictions fully fixed by energy losses and spatial diffusion in this configuration. In the particular case of DM annihilation in the e^+e^- channel, the prediction of the peak in $E^2\phi_{e^\pm}$ occurring at the WIMP mass (see Fig. 2), which determines the Voyager bounds on $\langle\sigma v\rangle$, further allows to get rid of spatial diffusion and relies only on rather well controlled local parameters (local dark matter and interstellar gas densities). This asymptotic peak prediction is therefore insensitive to uncertainties in the propagation parameters in this weak-reacceleration configuration, which seems to be favored by the most recent B/C data [37].

2. Constraints on dark matter decay

In this section, we conduct the same analysis as above but for decaying DM particles. The positron injection rate at position \vec{x} is $\propto \Gamma_\chi \rho(\vec{x})/m_\chi$, where $\Gamma_\chi = 1/\tau_\chi$ is the decay rate (τ_χ is the DM particle lifetime), and where we notice the linear dependence in the DM mass density profile, in contrast to the quadratic dependence that characterizes the annihilation rate. Our lower bounds for the lifetime are reported in Fig. 5, based on the same conservative assumptions as those used to derive our limits on the annihilation cross section (see right panel of Fig. 3).

-
- [1] J. R. Bond, A. S. Szalay, and M. S. Turner, *Physical Review Letters* **48**, 1636 (1982).
 - [2] S. Colombi, S. Dodelson, and L. M. Widrow, *Astrophys. J.* **458**, 1 (1996), [astro-ph/9505029](#).
 - [3] M. Viel, J. Lesgourgues, M. G. Haehnelt, S. Matarrese, and A. Riotto, *Phys. Rev. D* **71**, 063534 (2005), [astro-ph/0501562](#).
 - [4] M. Viel, G. D. Becker, J. S. Bolton, and M. G. Haehnelt, *Phys. Rev. D* **88**, 043502 (2013), [arXiv:1306.2314 \[astro-ph.CO\]](#).
 - [5] S. Bose, W. A. Hellwing, C. S. Frenk, A. Jenkins, M. R. Lovell, J. C. Helly, and B. Li, *MNRAS* **455**, 318 (2016), [arXiv:1507.01998](#).
 - [6] C. Boehm, T. A. Enßlin, and J. Silk, *Journal of Physics G Nuclear Physics* **30**, 279 (2004), [astro-ph/0208458](#).
 - [7] C. Boehm, J. A. Schewtschenko, R. J. Wilkinson, C. M. Baugh, and S. Pascoli, *MNRAS* **445**, L31 (2014), [arXiv:1404.7012](#).
 - [8] M. Boylan-Kolchin, J. S. Bullock, and M. Kaplinghat, *MNRAS* **415**, L40 (2011), [arXiv:1103.0007 \[astro-ph.CO\]](#).

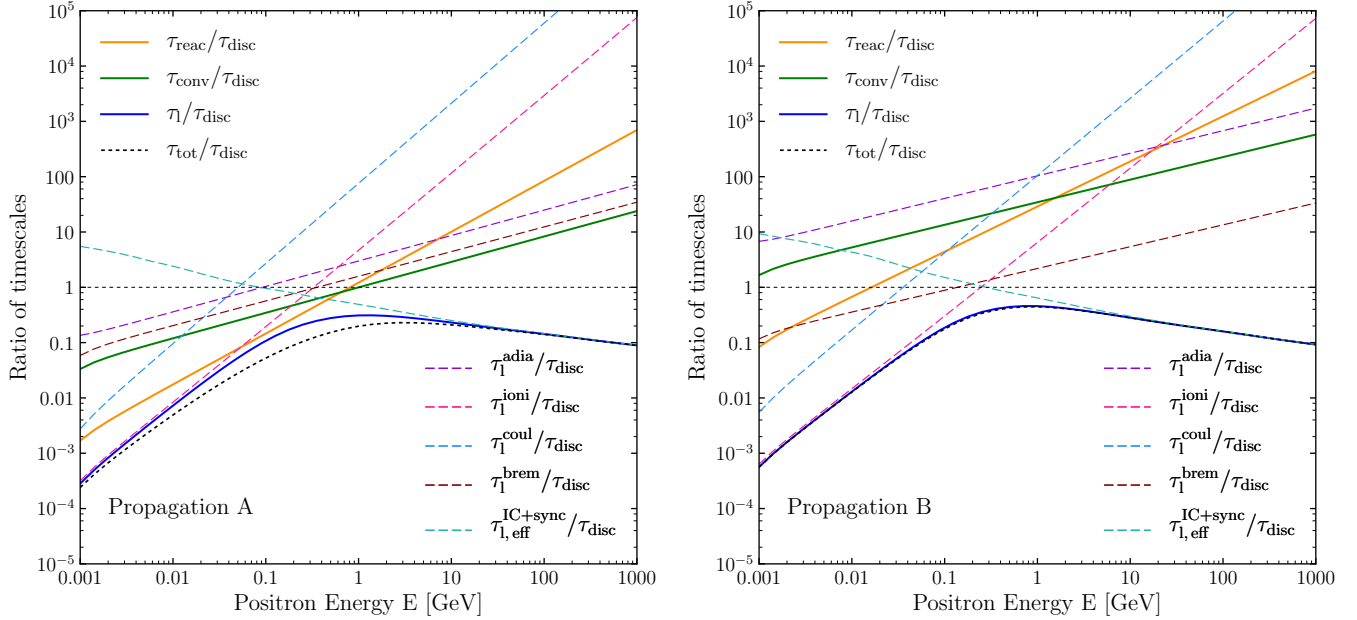


FIG. 4: Left panel: time scales associated with the different propagation processes of model A. Right panel: the same for model B.

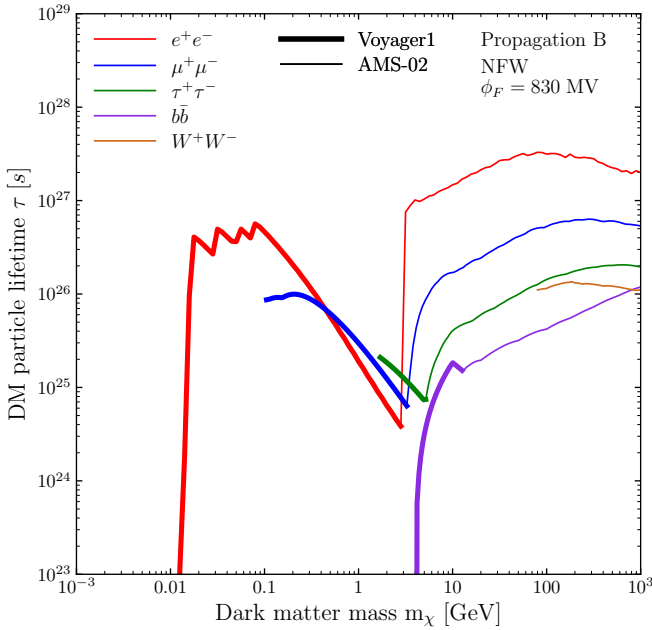


FIG. 5: Limits on the DM particle lifetime as a function of the DM particle m_χ . This figure assumes the same (conservative) model configuration as in the right panel of Fig. 3.

[9] X. Chu, C. Garcia-Cely, and T. Hambye, ArXiv e-prints (2016), [arXiv:1609.00399 \[hep-ph\]](#).
 [10] Y. Hochberg, E. Kuflik, T. Volansky, and J. G. Wacker, *Physical Review Letters* **113**, 171301 (2014), [arXiv:1402.5143 \[hep-ph\]](#).

[11] J. Alexander *et al.*, ArXiv e-prints (2016), [arXiv:1608.08632 \[hep-ph\]](#).
 [12] J. F. Beacom, N. F. Bell, and G. Bertone, *Physical Review Letters* **94**, 171301 (2005), [astro-ph/0409403](#).
 [13] R. Essig, E. Kuflik, S. D. McDermott, T. Volansky, and K. M. Zurek, *Journal of High Energy Physics* **11**, 193 (2013), [arXiv:1309.4091 \[hep-ph\]](#).
 [14] X. Chen and M. Kamionkowski, *Phys. Rev. D* **70**, 043502 (2004), [astro-ph/0310473](#).
 [15] T. R. Slatyer, *Phys. Rev. D* **93**, 023527 (2016), [arXiv:1506.03811 \[hep-ph\]](#).
 [16] H. Liu, T. R. Slatyer, and J. Zavala, *Phys. Rev. D* **94**, 063507 (2016), [arXiv:1604.02457](#).
 [17] J. Lavalle and P. Salati, *Comptes Rendus Physique* **13**, 740 (2012), [arXiv:1205.1004 \[astro-ph.HE\]](#).
 [18] L. J. Gleeson and W. I. Axford, *Astrophys. J.* **154**, 1011 (1968).
 [19] M. Potgieter, *Living Reviews in Solar Physics* **10**, 3 (2013), [arXiv:1306.4421 \[physics.space-ph\]](#).
 [20] A. C. Cummings, E. C. Stone, B. C. Heikkila, N. Lal, W. R. Webber, G. Jóhannesson, I. V. Moskalenko, E. Orlando, and T. A. Porter, *Astrophys. J.* **831**, 18 (2016).
 [21] S. M. Krimigis, C. O. Bostrom, T. P. Armstrong, W. I. Axford, C. Y. Fan, G. Gloeckler, and L. J. Lanzerotti, *Space Science Reviews* **21**, 329 (1977).
 [22] E. C. Stone, A. C. Cummings, F. B. McDonald, B. C. Heikkila, N. Lal, and W. R. Webber, *Science* **341**, 150 (2013).
 [23] M. Aguilar *et al.*, *Physical Review Letters* **113**, 121102 (2014).
 [24] D. Maurin, F. Melot, and R. Taillet, *Astron. Astroph.* **569**, A32 (2014), [arXiv:1302.5525 \[astro-ph.HE\]](#).
 [25] V. L. Ginzburg and S. I. Syrovatskii, *The Origin of Cosmic Rays*, New York: Macmillan, 1964 (1964).
 [26] S. V. Bulanov and V. A. Dogel, *Astrophysics and Space Science* **29**, 305 (1974).

- [27] I. V. Moskalenko and A. W. Strong, *Astrophys. J.* **493**, 694 (1998), [astro-ph/9710124](#).
- [28] T. Delahaye, R. Lineros, F. Donato, N. Fornengo, J. Lavalle, P. Salati, and R. Taillet, *Astron. Astroph.* **501**, 821 (2009), [arXiv:0809.5268](#).
- [29] T. Delahaye, J. Lavalle, R. Lineros, F. Donato, and N. Fornengo, *Astron. Astroph.* **524**, A51 (2010), [arXiv:1002.1910 \[astro-ph.HE\]](#).
- [30] M. Boudaud, S. Aupetit, S. Caroff, A. Putze, G. Belanger, Y. Genolini, C. Goy, V. Poireau, V. Poulin, S. Rosier, P. Salati, L. Tao, and M. Vecchi, *Astron. Astroph.* **575**, A67 (2015), [arXiv:1410.3799 \[astro-ph.HE\]](#).
- [31] M. Boudaud, E. F. Bueno, S. Caroff, Y. Genolini, V. Poulin, V. Poireau, A. Putze, S. Rosier, P. Salati, and M. Vecchi, *ArXiv e-prints* (2016), [arXiv:1612.03924 \[astro-ph.HE\]](#).
- [32] D. Maurin, F. Donato, R. Taillet, and P. Salati, *Astrophys. J.* **555**, 585 (2001), [astro-ph/0101231](#).
- [33] A. W. Strong and I. V. Moskalenko, *Astrophys. J.* **509**, 212 (1998), [astro-ph/9807150](#).
- [34] C. Evoli, D. Gaggero, D. Grasso, and L. Maccione, *JCAP* **10**, 018 (2008), [arXiv:0807.4730](#).
- [35] R. Kissmann, *Astroparticle Physics* **55**, 37 (2014), [arXiv:1401.4035 \[astro-ph.HE\]](#).
- [36] J. Lavalle, D. Maurin, and A. Putze, *Phys. Rev. D* **90**, 081301 (2014), [arXiv:1407.2540 \[astro-ph.HE\]](#).
- [37] R. Kappl, A. Reinert, and M. W. Winkler, *JCAP* **10**, 034 (2015), [arXiv:1506.04145 \[astro-ph.HE\]](#).
- [38] F. Donato, N. Fornengo, D. Maurin, P. Salati, and R. Taillet, *Phys. Rev. D* **69**, 063501 (2004), [astro-ph/0306207](#).
- [39] C. S. Shen, *Astrophys. J. Lett.* **162**, L181+ (1970).
- [40] F. A. Aharonian, A. M. Atoyan, and H. J. Voelk, *Astron. Astroph.* **294**, L41 (1995).
- [41] L. A. Fisk, *J. Geophys. Res.* **76**, 221 (1971).
- [42] A. Ghelfi, F. Barao, L. Derome, and D. Maurin, *Astron. Astroph.* **591**, A94 (2016), [arXiv:1511.08650 \[astro-ph.HE\]](#).
- [43] A. Thornbury and L. O. Drury, *MNRAS* **442**, 3010 (2014), [arXiv:1404.2104 \[astro-ph.HE\]](#).
- [44] L. O. Drury and A. W. Strong, *Astron. Astroph.* **597**, A117 (2017), [arXiv:1608.04227 \[astro-ph.HE\]](#).
- [45] G. Bélanger, F. Boudjema, A. Pukhov, and A. Semenov, *Computer Physics Communications* **192**, 322 (2015), [arXiv:1407.6129 \[hep-ph\]](#).
- [46] J. F. Navarro, C. S. Frenk, and S. D. M. White, *Astrophys. J.* **490**, 493 (1997), [astro-ph/9611107](#).
- [47] P. J. McMillan, *MNRAS* **465**, 76 (2017), [arXiv:1608.00971](#).
- [48] K. M. Ferrière, *Reviews of Modern Physics* **73**, 1031 (2001), [astro-ph/0106359](#).
- [49] H. Nakanishi and Y. Sofue, *Pub. Astron. Soc. Jap.* **55**, 191 (2003), [astro-ph/0304338](#).
- [50] L. Bergström, T. Bringmann, I. Cholis, D. Hooper, and C. Weniger, *Physical Review Letters* **111**, 171101 (2013), [arXiv:1306.3983 \[astro-ph.HE\]](#).
- [51] M. J. Reid, K. M. Menten, A. Brunthaler, X. W. Zheng, T. M. Dame, Y. Xu, Y. Wu, B. Zhang, A. Sanna, M. Sato, K. Hachisuka, Y. K. Choi, K. Immer, L. Moscadelli, K. L. J. Rygl, and A. Bartkiewicz, *Astrophys. J.* **783**, 130 (2014), [arXiv:1401.5377 \[astro-ph.GA\]](#).
- [52] D. P. Finkbeiner and N. Weiner, *Phys. Rev. D* **76**, 083519 (2007), [astro-ph/0702587](#).